Superconducting gap and nematic resonance at the quantum critical point observed by Raman scattering in $BaFe_2(As_{1-x}P_x)_2$

T. Adachi [1,*] M. Nakajima,[1] Y. Gallais,[2] S. Miyasaka [1] and S. Tajima[1]

[1]*Department of Physics, Graduate School of Science, Osaka University, Toyonaka, Osaka 560-0043, Japan*

[2]*Laboratoire Matériaux et Phénomènes Quantiques (UMR 7162 CNRS), Université de Paris, Bat. Condorcet, 75205 Paris Cedex 13, France*

(Received 7 December 2019; revised manuscript received 21 January 2020; accepted 22 January 2020; published 3 February 2020)

We report comprehensive temperature and doping dependences of the Raman scattering spectra for $BaFe_2(As_{1-x}P_x)_2$ ($x = 0, 0.07, 0.24, 0.32$, and 0.38), focusing on the nematic fluctuation and the superconducting responses. With increasing x, the bare nematic transition temperature estimated from the Raman spectra reaches $T = 0$ K at the optimal doping, which indicates a quantum critical point (QCP) at this composition. In the superconducting compositions, in addition to the pair-breaking peaks observed in the A_{1g} and B_{1g} spectra, another strong B_{1g} peak appears below the superconducting transition temperature, which is ascribed to the nematic resonance peak. The observation of this peak indicates significant nematic correlations in the superconducting state near the QCP in this compound.

DOI: 10.1103/PhysRevB.101.085102

I. INTRODUCTION

More than a decade has passed since the discovery of iron-based superconductors (IBSs) [1]. However, its superconducting (SC) mechanism is not yet well understood. A smoking gun is the fact that a magnetic ordered phase is adjacent to the SC phase, and thus the spin fluctuation is a strong candidate for the pairing glue. On the other hand, recently nematic fluctuations have also been observed [2–11], which have attracted much attention. Several theoretical and experimental studies suggest that nematic fluctuations may play a key role in the superconductivity in IBSs [12–18]. However, whether or not nematic quantum criticality is relevant for the appearance of superconductivity in IBS remains largely unsettled.

Raman scattering spectroscopy is a powerful tool to investigate the electronic properties in solids. In particular, the symmetry-resolved sensitivity enables us to directly access nematic behavior without any external field such as uniaxial strain. Recently, Raman scattering experiments have been performed on many IBSs such as $Ba(Fe_{1-x}Co_x)_2As_2$, $NaFe_{1-x}Co_xAs$, FeSe, and LaFeAsO [11,19–21]. These results indicate that there exist nematic fluctuations in the tetragonal phase of several IBSs. From the doping dependence of Raman scattering spectra in $Ba(Fe_{1-x}Co_x)_2As_2$ and $NaFe_{1-x}Co_xAs$, a nematic quantum critical point (QCP) has been revealed near the magnetic critical point close to the optimal superconducting transition temperature (T_c) [11,21,22]. Moreover, for the superconducting $Ba(Fe_{1-x}Co_x)_2As_2$, a nematic resonance mode was observed below the SC gap energies near the nematic QCP [23]. A similar peak seen in $NaFe_{1-x}Co_xAs$ was attributed to an in-gap collective mode in the nematic channel, consistent with the nematic resonance scenario [21]. In $Ba(Fe_{1-x}Co_x)_2As_2$, however, one concern is that SC gap features in the Raman scattering spectra of the nonnematic channel are weak [24], likely due to the disorder effects introduced by Co substitution for Fe.

Here we have chosen the $BaFe_2(As_{1-x}P_x)_2$ system, because it is considered to be a less disordered system than $Ba(Fe_{1-x}Co_x)_2As_2$ [25,26], and clear fingerprints of quantum criticality have been observed in thermodynamic measurements [27–29]. Therefore, it is an attractive system for the study of nematic fluctuations and related phenomena, but so far no systematic Raman scattering study has been reported on this compound.

Here, we present a systematic study of Raman scattering on $BaFe_2(As_{1-x}P_x)_2$ over a wide range of P compositions (xs). At all the studied compositions, nematic fluctuations are observed above the structural transition temperature (T_s) or T_c. The bare nematic transition temperature T_0 reaches 0 K near the optimal doping, which implies the existence of a nematic QCP at this composition. In the SC state, a clear pair-breaking (PB) peak is observed in the A_{1g} symmetry for $x = 0.32$ and 0.38. It is ascribed to the SC gap of the hole pockets. Moreover, another strong peak is observed in the B_{1g} symmetry towards the nematic QCP. This peak is ascribed to the nematic resonance peak, indicating the persistence of significant nematic correlations in the SC state near the QCP.

II. METHODS

Single crystals of $BaFe_2(As_{1-x}P_x)_2$ ($x = 0$, 0.07, 0.24, 0.32, and 0.38) were grown by a self-flux method as described elsewhere [30]. The transition temperatures (T_s and T_c) were determined by resistivity measurements before Raman scattering measurements. Single crystals were cleaved just before being loaded into a cryostat. Raman scattering spectra were

*t.adachi63@gmail.com

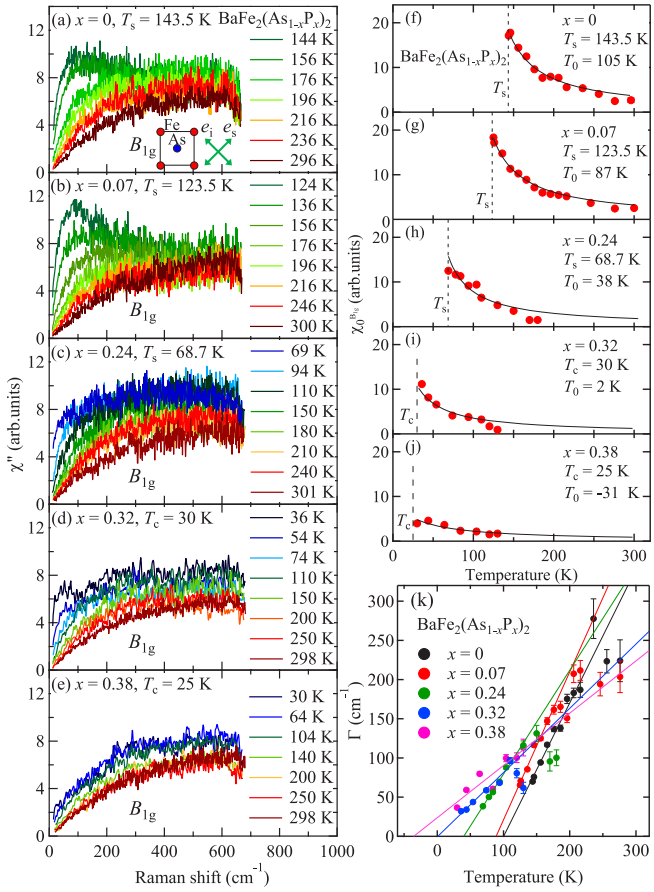

FIG. 1. (a)–(e) Temperature dependence of B_{1g} Raman scattering spectra for $x = 0$, 0.07, 0.24, 0.32, and 0.38. (f)–(j) Temperature dependence of the Raman susceptibility, $\chi_0^{B_{1g}}$, of BaFe$_2$(As$_{1-x}$P$_x$)$_2$ ($x = 0$, 0.07, 0.24, 0.32, and 0.38). (k) Temperature dependence of the scattering rate Γ for $x = 0$, 0.07, 0.24, 0.32, and 0.38.

obtained in the pseudo-backscattering configuration using an Ar laser line (514.5 nm) and a T64000 Jobin-Yvon triple grating spectrometer equipped with a liquid-nitrogen-cooled charge-coupled device detector. The gratings have a density of 1800 g/mm. For measurements below T_c, the laser power was set to 4 mW, while it was 10 mW for measurements above T_c. The laser heating under these conditions was estimated to be 4 and 6–10 K, respectively.

$A_{1g} + B_{2g}$, B_{1g}, and B_{2g} Raman spectra were measured with the incident (i) and scattered (s) light polarizations of $(i, s) = (x, x)$, (x, y), and (x, y), respectively. Here, x and y are oriented along the directions of Fe-Fe bonds, while x' and y' are along the diagonals of Fe-Fe bonds. The pure A_{1g} spectrum is obtained by subtraction of the xy spectrum from the $x'x'$ one.

III. RESULTS AND DISCUSSION

First, we discuss the nematic fluctuations above T_s. Figures 1(a)–1(e) show the temperature dependence of the B_{1g} Raman responses for BaFe$_2$(As$_{1-x}$P$_x$)$_2$ ($x = 0$, 0.07, 0.24, 0.32, and 0.38). For all samples, the Raman intensity displays a strong enhancement at low energies upon cooling towards T_s or T_c. This enhancement is suppressed below T_s or T_c and is not observed in the A_{1g} and B_{2g} symmetries (see Figs. 5 and 6 in Appendixes A and B). A similar behavior has been reported also in some other IBSs and is attributed to enhanced $d_{x^2-y^2}$ charge fluctuations, namely, nematic fluctuations, near T_s [31]. The B_{1g} Raman response at low frequencies near T_s is well reproduced using a quasielastic peak (QEP) lineshape, $\chi''_{\rm QEP}$, expressed by

$$\chi''_{\rm QEP} = \frac{A\omega\Gamma}{\omega^2 + \Gamma^2}, \tag{1}$$

where A is a constant and Γ can be interpreted as a quasiparticle scattering rate renormalized by nematic correlations [31]. In addition to this QEP, a temperature-independent ω-linear background was assumed. The QEP of the B_{1g} Raman scattering response is directly connected with the static charge nematic susceptibility, $\chi_0^{B_{1g}}$ via the Kramers-Kronig relation,

$$\chi_0^{B_{1g}} = \frac{2}{\pi}\int_0^\infty \frac{\chi''_{\rm QEP}}{\omega} d\omega. \tag{2}$$

Within a mean-field theory framework, we expect $\chi_0^{B_{1g}}$ to follow Curie-Weiss behavior,

$$\chi_0^{B_{1g}} = \frac{C}{T - T_0}, \tag{3}$$

where C is a constant and T_0 is the charge nematic transition temperature.

Figures 1(f)–1(j) present the temperature dependence of $\chi_0^{B_{1g}}$ obtained from the data in Figs. 1(a)–1(e) (see Fig. 7 in Appendix C). At each P composition x, the data are well fitted to the Curie-Weiss curve as long as the temperature is near T_s ($T \leqslant T_s + 70$ K).

For all the samples, T_0 is always lower than T_s, consistent with previous results on Ba(Fe$_{1-x}$Co$_x$)$_2$As$_2$ [11]. This is expected because Raman scattering probes the nematic susceptibility in the dynamical limit. The static nematic susceptibility extracted in this limit does not couple to the soft orthorhombic acoustical phonon and can, thus, be considered as the bare lattice-free nematic susceptibility [31,33]. This was confirmed in Ba(Fe$_{1-x}$Co$_x$)$_2$As$_2$ by comparing the nematic susceptibility and the shear modulus Cs [11,32,33]. Figure 1(k) shows the temperature dependence of the linewidth (Γ) of the QEP in Eq. (1). Γ decreases as the temperature approaches T_s or T_c. In the mean-field theory of Raman scattering near a nematic instability [31], this parameter is the quasiparticle scattering rate Γ_0 renormalized by the nematic correlation length. Assuming a weakly T dependent Γ_0 near T_s, $1/\Gamma$ should follow a Curie-Weiss temperature dependence near T_s and vanishes at T_0. Therefore, another estimate of T_0 can be deduced by extrapolating the T-linear fitting line for Γ. The obtained T_0 values are in broad agreement with those deduced from $\chi_0^{B_{1g}}$ in Figs. 1(f)–1(j).

The T_0 for BaFe$_2$As$_2$ in this study is in good agreement with the previous study [11] and the shear modulus study [32], whereas it is lower than that obtained by the elastoresistance experiment [2]. It has been reported that elastoresistance experiments tend to give higher T_0 values than Raman scattering and shear modulus ones for reasons which are not clear at present [34].

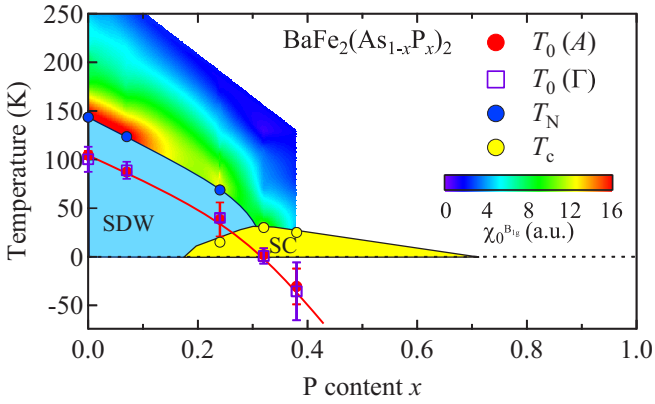

FIG. 2. Phase diagram of $BaFe_2(As_{1-x}P_x)_2$. The magnetic phase transition temperature (T_N) and T_c are taken from Ref. [30]. The filled red circle indicates T_0 derived from the area (A) of the QEP, while the open purple square indicates T_0 derived from the width (Γ) of the QEP. The color plot indicates the strength of the $\chi_0^{B_{1g}}$.

In Fig. 2, the estimated T_0 and $\chi_0^{B_{1g}}$ are plotted in the phase diagram of $BaFe_2(As_{1-x}P_x)_2$ obtained in the previous studies [30]. The color plot indicates the strength of the $\chi_0^{B_{1g}}$. T_0 reaches 0 K around the optimal doping ($x = 0.32$), indicating a nematic QCP. A similar result was reported by the elastoresistance experiment [35].

Next, we discuss the Raman responses in the SC state. The temperature dependences of the A_{1g} and B_{1g} Raman scattering spectra below T_c were precisely measured for $x = 0.32$ and 0.38. As for the B_{2g} Raman response, no spectral difference was observed between above and below T_c. As shown in Figs. 3(a) and 3(b), in both of the A_{1g} and B_{1g} symmetries, distinct features derived from superconductivity are observed. Figure 3(a) demonstrates that a peak develops with decreasing temperature. The A_{1g} peak energy $\Omega_{A_{1g}}$ at 8 K is about 108 cm^{-1}–13.4 meV. This energy is comparable to the angle-resolved photoemission spectroscopy (ARPES) data, $2\Delta_{hole}$–14 meV, where Δ_{hole} is the averaged SC gap of hole pockets [36]. Therefore, we assign this peak to the PB peak derived from the gap opening on the hole pockets. The A_{1g} spectral shapes near the lowest frequency are almost flat, suggesting a full gap on the hole pockets. Note that the peak around 200 cm^{-1} observed in this symmetry exists already in the normal state.

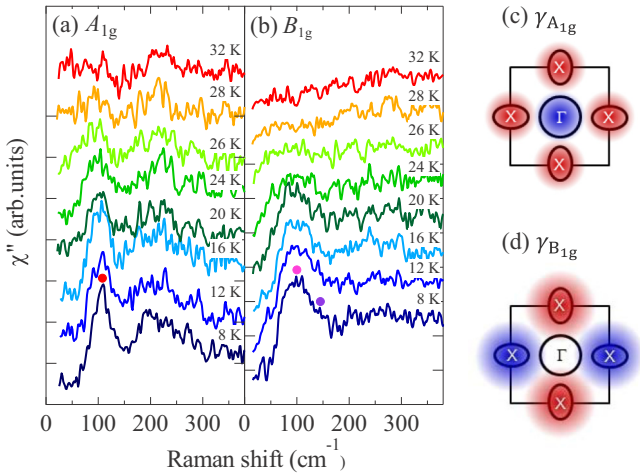

FIG. 3. (a), (b) Raman scattering spectra in A_{1g} and B_{1g} symmetries of $BaFe_2(As_{1-x}P_x)_2$ ($x = 0.32$, $T_c = 30$ K) at low temperatures. From the bottom (the lowest temperature) to the top (near T_c), each spectrum is plotted with each offset. (c), (d) Raman vertices for A_{1g} and B_{1g} symmetries. Red and blue colors indicate positive and negative values, respectively. The Raman vertex for A_{1g} symmetry is illustrated according to the result of the effective-mass approximation [37,38].

As shown in Fig. 3(b), the spectral shapes in the B_{1g} symmetry are apparently similar to those in the A_{1g} symmetry. In the B_{1g} symmetry, a distinct peak grows around 100 cm^{-1} at low temperatures. As the peak energy $\Omega^L_{B_{1g}}$ is close to $\Omega_{A_{1g}}$, one may consider that it is a PB peak derived from the hole pockets. However, it is unlikely because the B_{1g} form factor is expected to probe dominantly the electron pockets, as illustrated in Fig. 3(d) [37,38]. Instead, the weak shoulder structure indicated by the purple mark around 145 cm^{-1} (~18 meV) might be a more appropriate candidate of the B_{1g} PB peak, because its energy $\Omega^H_{B_{1g}}$ is close to $2\Delta_{electron}$ in ARPES [36].

Figures 4(a) and 4(b) compare the subtracted Raman spectra ($\chi''_{SC} - \chi''_N$) for $x = 0.32$ and 0.38 in A_{1g} and B_{1g} symmetries, where χ''_{SC} and χ''_N is the Raman susceptibility at 8 K and the temperature just above T_c, respectively. In the A_{1g} spectra, one can clearly see that $\Omega_{A_{1g}}$ decreases with doping, namely, with decreasing T_c. While the spectral weight of the A_{1g} peak slightly decreases with doping, that of B_{1g} at $\Omega^L_{B_{1g}}$ is strongly suppressed with increasing x. This tendency of an intensity decrease with doping continues to the strongly overdoped region [39]. At $x = 0.5$, the PB peak in the A_{1g} symmetry is clearly observed, while the B_{1g} spectrum does not show any distinct peak.

The doping dependences of the peak intensities in ($\chi''_{SC} - \chi''_N$) are shown in Fig. 4(c). The data for $x = 0.50$ [39] were normalized with our data at 200 cm^{-1}. The PB peak area is proportional to the density of Cooper pairs weighted by the square of the Raman vertex in the BCS framework [40]. In fact, the doping dependence of the A_{1g} peak area follows that of the superfluid density $n_s(0)$ obtained by the specific heat measurement [41]. This is because the specific heat observes mainly heavy quasiparticles, which are generally located in the hole bands responsible for the A_{1g} PB peak.

The behavior of the B_{1g} peak is, however, very different from that of the A_{1g} peak. The B_{1g} peak intensity of $x = 0.32$ is almost four times larger than that of $x = 0.38$, while the T_c of $x = 0.32$ (=30 K) is only 5 K higher than that of $x = 0.38$ (=25 K). The enhancement of the B_{1g} peak intensity towards the nematic QCP has also been observed in $NaFe_{1-x}Co_xAs$ and $Ba(Fe_{1-x}Co_x)_2As_2$ [21,23,42]. Recently, Gallais *et al.* pointed out that sufficiently close to a nematic QCP the B_{1g} PB peak can be transformed into a nematic resonance mode which arises due to nematic correlations between quasiparticles [23]. According to this theory, the bare PB peak intensity at $\omega = 2\Delta$ gradually decreases close to the QCP and the nematic resonance peak appears at an energy Ω_r lower than 2Δ.

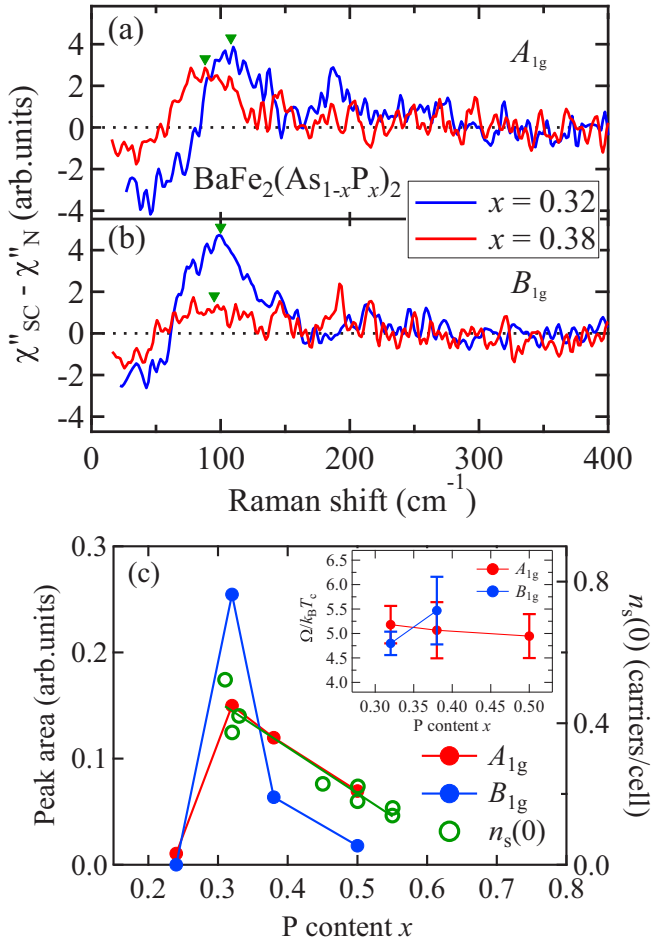

FIG. 4. (a), (b) Subtracted Raman scattering spectra ($\chi''_{SC} - \chi''_N$) in A_{1g} and B_{1g} symmetries of $BaFe_2(As_{1-x}P_x)_2$ ($x = 0.32$ and 0.38). Green triangles indicate peak energies of peaks. (c) Doping dependence of the peak area at $\Omega_{A_{1g}}$ and $\Omega^L_{B_{1g}}$ and $n_s(0)$ estimated from the specific heat [41]. Inset: Doping dependence of the peak energy (Ω) divided by k_BT_c in A_{1g} and B_{1g} symmetries. The data at $x = 0.50$ are taken from Ref. [39].

This scenario is in good agreement with the present result in the following senses. (i) The peak energy at $\Omega^L_{B_{1g}}$ is lower than 2Δ on the electron pockets observed in the present study as well as the ARPES experiment [36]. (ii) The transformation from the PB peak to the nematic resonance also explains naturally the strong enhancement of the B_{1g} peak intensity towards the QCP. (iii) Although with increasing x the B_{1g} peak becomes too weak and broad to discuss its T_c scaling, $\Omega^L_{B_{1g}}$ does not seem to scale with T_c, while $\Omega_{A_{1g}}$ almost does as shown in the inset in Fig. 4(c). It is the same trend as with $Ba(Fe_{1-x}Co_x)_2As_2$ and consistent with the theory [23]. (iv) Importantly the nematic quantum critical behavior was observed only for the B_{1g} peak at $\Omega^L_{B_{1g}}$, and not for the other PB peaks, which represents an intrinsic feature of nematicity.

It should be noted that a nematic resonance is expected to arise irrespective of the microscopic origin of nematicity such as charge (Pomeranchuk instability) [43,44] or orbital [45,46] or spin [47–49]. Whatever the origin of nematic fluctuations is, the presence of a nematic resonance mode within a SC gap and its enhancement towards the QCP strongly suggest a close relation between the nematic fluctuation and superconductivity. An intriguing question is whether these enhanced nematic correlations deep in the SC state can play a role in the divergentlike behavior observed in the London penetration depth of $BaFe_2(As_{1-x}P_x)_2$ close to the QCP, near $x = 0.3$ [28].

IV. CONCLUSION

In conclusion, we have systematically investigated the Raman scattering spectra for $BaFe_2(As_{1-x}P_x)_2$ ($x = 0$, 0.07, 0.24, 0.32, and 0.38). The nematic fluctuations above T_s or T_c were observed at all the studied compositions including the SC ones. The bare nematic transition temperature T_0 becomes 0 K near the optimal doping ($x = 0.32$), indicating the existence of a nematic QCP. In the SC state at $x = 0.32$ and 0.38, in addition to the pair-breaking peaks for the gaps on the hole and electron pockets, we observed a strong B_{1g} peak that is much stronger than the PB peak and correlates with the normal state nematic fluctuations (i.e., QCP behavior). From its doping- and symmetry-dependent behaviors, this peak can be ascribed to a nematic resonance mode. The present results strongly suggest a firm relation between the superconductivity and the nematic fluctuation in this compound.

ACKNOWLEDGMENTS

This work was supported by Grants-in-Aid for Scientific Research from JSPS, Japan. T.A. acknowledges the Grant-in-Aid for JSPS Fellows Grant No. 15J01811.

APPENDIX A: A_{1g} AND B_{2g} SPECTRA

Figure 5 shows the temperature dependence of the $A_{1g} + B_{2g}$ and B_{2g} Raman responses for $BaFe_2(As_{1-x}P_x)_2$ ($x = 0$, 0.24). In our measurements, no hump structures could be observed in the A_{1g} and B_{2g} symmetries above T_s for all the studied compositions. Moreover, there is almost no temperature dependence of the spectra in these symmetries above T_s.

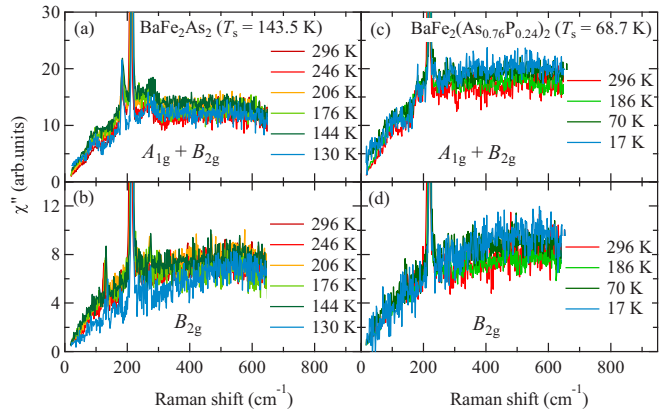

FIG. 5. Temperature dependence of the $A_{1g} + B_{2g}$ and B_{2g} Raman scattering spectra for $BaFe_2(As_{1-x}P_x)_2$ ($x = 0$ and 0.24).

APPENDIX B: B_{1g} SPECTRA AROUND T_s

The B_{1g} spectra above and below T_s are presented in Fig. 6. The hump structure rapidly disappears when the sample experiences the structural transition to the low-temperature orthorhombic phase, while it increases with decreasing temperature at $T > T_s$. It is noted that the sharp peak around 180 cm^{-1} below T_s is the A_g phonon mode, which is the same as the A_{1g} phonon mode seen in the tetragonal phase. It can be observed in the $x'y'$ polarization configuration only in the orthorhombic phase.

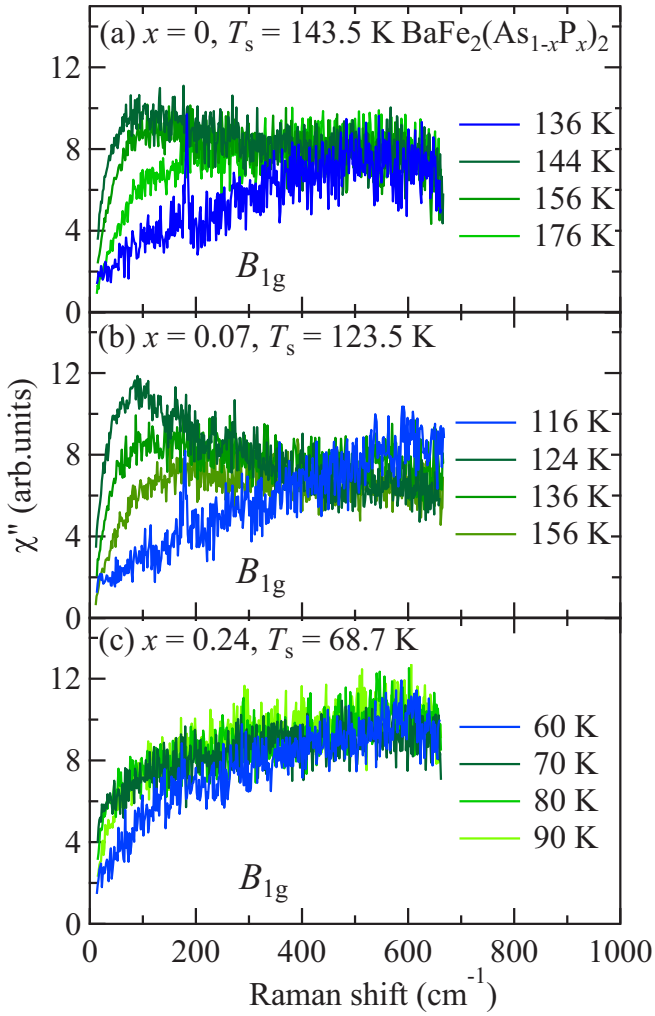

FIG. 6. Temperature dependence of the B_{1g} Raman scattering spectra for $BaFe_2(As_{1-x}P_x)_2$ ($x = 0$, 0.07, and 0.24).

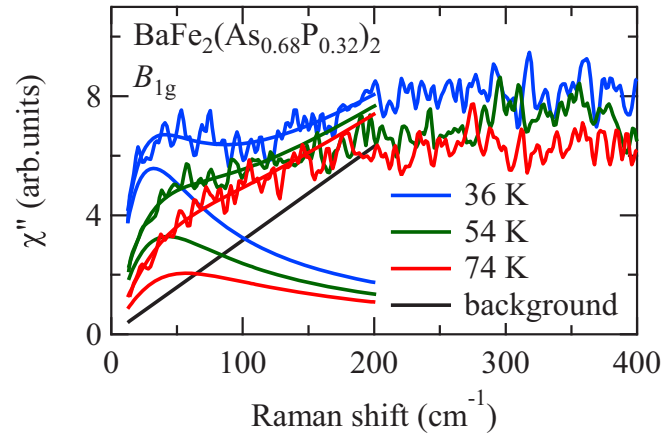

FIG. 7. Fits of the B_{1g} Raman responses at several temperatures for $BaFe_2(As_{0.68}P_{0.32})_2$. Each fitted line is decomposed into the QEP at each temperature and the background.

APPENDIX C: DETERMINATION OF T_0

In our analysis, we assumed that the electronic background in the B_{1g} Raman response is T independent in the same manner as in the previous study [11]. Then we can decompose the B_{1g} Raman response into the quasielastic peak and the temperature-independent ω-linear background as long as the temperature is near T_s ($T \leqslant T_s + 70$ K) and the frequency is lower than 200 cm^{-1}. Figure 7 presents B_{1g} Raman responses and fitted lines at several temperatures for $BaFe_2(As_{0.68}P_{0.32})_2$. The B_{1g} Raman responses at low frequencies are well reproduced by this fitting and the nematic susceptibility can be extracted.

[1] Y. Kamihara, T. Watanabe, M. Hirano, and H. Hosono, J. Am. Chem. Soc. **130**, 3296 (2008).

[2] J.-H. Chu, H.-H. Kuo, J. G. Analytis, and I. R. Fisher, Science **337**, 710 (2012).

[3] A. Patz, T. Li, S. Ran, R. M. Fernandes, J. Schmalian, S. L. Bud'ko, P. C. Canfield, I. E. Perakis, and J. Wang, Nat. Commun. **5**, 3229 (2014).

[4] A. E. Böhmer, P. Burger, F. Hardy, T. Wolf, P. Schweiss, R. Fromknecht, M. Reinecker, W. Schranz, and C. Meingast, Phys. Rev. Lett **112**, 047001 (2014).

[5] X. Lu, J. T. Park, R. Zhang, H. Luo, A. H. Nevidomskyy, Q. Si, and P. Dai, Science **345**, 657 (2014).

[6] C. Mirri, A. Dusza, S. Bastelberger, M. Chinotti, L. Degiorgi, J.-H. Chu, H.-H. Kuo, and I. R. Fisher, Phys. Rev. Lett. **115**, 107001 (2015).

[7] A. E. Böhmer, T. Arai, F. Hardy, T. Hattori, T. Iye, T. Wolf, H. v. Löhneysen, K. Ishida, and C. Meingast, Phys. Rev. Lett. **114**, 027001 (2015).

[8] A. P. Dioguardi, T. Kissikov, C. H. Lin, K. R. Shirer, M. M. Lawson, H.-J. Grafe, J.-H. Chu, I. R. Fisher, R. M. Fernandes, and N. J. Curro, Phys. Rev. Lett **116**, 107202 (2016).

[9] S. Hosoi, K. Matsuura, K. Ishida, H. Wang, Y. Mizukami, T. Watashige, S. Kasahara, Y. Matsuda, and T. Shibauchi, Proc. Natl. Acad. Sci. USA **113**, 8139 (2016).

[10] M. Toyoda, Y. Kobayashi, and M. Itoh, Phys. Rev. B **97**, 094515 (2018).
[11] Y. Gallais, R. M. Fernandes, I. Paul, L. Chauviére, Y.-X. Yang, M.-A. Méasson, M. Cazayous, A. Sacuto, D. Colson, and A. Forget, Phys. Rev. Lett. **111**, 267001 (2013).
[12] Z. Liu, T. Xie, D. Gong, X. Ma, R. M. Fernandes, Y.-F. Yang, H. Luo, and S. Li, J. Phys.: Condens. Matter **30**, 445604 (2018).
[13] H. Yamase and R. Zeyher, Phys. Rev. B **88**, 180502(R) (2013).
[14] S. Lederer, Y. Schattner, E. Berg, and S. A. Kivelson, Phys. Rev. Lett. **114**, 097001 (2015).
[15] T. Agatsuma and H. Yamase, Phys. Rev. B **94**, 214505 (2016).
[16] S. Lederer, Y. Schattner, E. Berg, and S. A. Kivelson, Proc. Natl. Acad. Sci. USA **114**, 4905 (2017).
[17] Y. Sato, S. Kasahara, T. Taniguchi, X. Z. Xing, Y. Kasahara, Y. Tokiwa, T. Shibauchi, and Y. Matsuda, Proc. Natl. Acad. Sci. USA **115**, 1227 (2018).
[18] D. Labat and I. Paul, Phys. Rev. B **96**, 195146 (2017).
[19] P. Massat, D. Farina, I. Paul, S. Karlsson, P. Strobel, P. Toulemonde, M.-A. Méasson, M. Cazayous, A. Sacuto, S. Kasahara, T. Shibauchi, Y. Matsuda, and Y. Gallais, Proc. Natl. Acad. Sci. USA **113**, 9177 (2016).
[20] U. F. Kaneko, P. F. Gomes, A. F. Garcéa-Flores, J.-Q. Yan, T. A. Lograsso, G. E. Barberis, D. Vaknin, and E. Granado, Phys. Rev. B **96**, 014506 (2017).
[21] V. K. Thorsmølle, M. Khodas, Z. P. Yin, C. Zhang, S. V. Carr, P. Dai, and G. Blumberg, Phys. Rev. B **93**, 054515 (2016).
[22] F. Kretzschmar, T. Böhm, U. Karahasanovic, B. Muschler, A. Baum, D. Jost, J. Schmalian, S. Caprara, M. Grilli, C. Di Castro, J. G. Analytis, J.-H. Chu, I. R. Fisher, and R. Hackl, Nat. Phys. **12**, 560 (2016).
[23] Y. Gallais, I. Paul, L. Chauviére, and J. Schmalian, Phys. Rev. Lett. **116**, 017001 (2016).
[24] T. Böhm, R. H. Ahangharnejhad, D. Jost, A. Baum, B. Muschler, F. Kretzschmar, P. Adelmann, T. Wolf, H.-H. Wen, J.-H. Chu, I. R. Fisher, and R. Hackl, Phys. Status Solidi B **254**, 1600308 (2017).
[25] S. Ishida, M. Nakajima, T. Liang, K. Kihou, C. H. Lee, A. Iyo, H. Eisaki, T. Kakeshita, Y. Tomioka, T. Ito, and S. Uchida, J. Am. Chem. Soc. **135**, 3158 (2013).
[26] M. Nakajima, M. Nagafuchi, and S. Tajima, Phys. Rev. B **97**, 094511 (2018).
[27] H. Shishido, A. F. Bangura, A. I. Coldea, S. Tonegawa, K. Hashimoto, S. Kasahara, P. M. C. Rourke, H. Ikeda, T. Terashima, R. Settai, Y. Ōnuki, D. Vignolles, C. Proust, B. Vignolle, A. McCollam, Y. Matsuda, T. Shibauchi, and A. Carrington, Phys. Rev. Lett. **104**, 057008 (2010).
[28] K. Hashimoto, K. Cho, T. Shibauchi, S. Kasahara, Y. Mizukami, R. Katsumata, Y. Tsuruhara, T. Terashima, H. Ikeda, M. A. Tanatar, H. Kitano, N. Salovich, R. W. Giannetta, P. Walmsley, A. Carrington, R. Prozorov, and Y. Matsuda, Science **336**, 1554 (2012).
[29] P. Walmsley, C. Putzke, L. Malone, I. Guillamón, D. Vignolles, C. Proust, S. Badoux, A. I. Coldea, M. D. Watson, S. Kasahara, Y. Mizukami, T. Shibauchi, Y. Matsuda, and A. Carrington, Phys. Rev. Lett. **110**, 257002 (2013).
[30] M. Nakajima, S. Uchida, K. Kihou, C. H. Lee, A. Iyo, and H. Eisaki, J. Phys. Soc. Jpn. **81**, 104710 (2012).
[31] Y. Gallais and I. Paul, C. R. Physique **17**, 113 (2016).
[32] M. Yoshizawa, D. Kimura, T. Chiba, S. Simayi, Y. Nakanishi, K. Kihou, C.-H. Lee, A. Iyo, H. Eisaki, M. Nakajima, and S. Uchida, J. Phys. Soc. Jpn. **81**, 024604 (2012).
[33] H. Kontani and Y. Yamakawa, Phys. Rev. Lett. **113**, 047001 (2014).
[34] A. E. Böhmer and C. Meingast, C. R. Phys. **17**, 90 (2016).
[35] H.-H. Kuo, J.-H. Chu, J. C. Palmstrom, S. A. Kivelson, and I. R. Fisher, Science **352**, 958 (2016).
[36] Y. Zhang, Z. R. Ye, Q. Q. Ge, F. Chen, Juan Jiang, M. Xu, B. P. Xie, and D. L. Feng, Nat. Phys. **8**, 371 (2012).
[37] I. I. Mazin, T. P. Devereaux, J. G. Analytis, J.-H. Chu, I. R. Fisher, B. Muschler, and R. Hackl, Phys. Rev. B **82**, 180502(R) (2010).
[38] T. Böhm, A. F. Kemper, B. Moritz, F. Kretzschmar, B. Muschler, H.-M. Eiter, R. Hackl, T. P. Devereaux, D. J. Scalapino, and Hai-Hu Wen, Phys. Rev. X **4**, 041046 (2014).
[39] S.-F. Wu, W.-L. Zhang, D. Hu, H.-H. Kung, A. Lee, H.-C. Mao, P.-C. Dai, H. Ding, P. Richard, and G. Blumberg, arXiv:1607.06575v1.
[40] S. Blanc, Y. Gallais, A. Sacuto, M. Cazayous, M. A. Méasson, G. D. Gu, J. S. Wen, and Z. J. Xu, Phys. Rev. B **80**, 140502(R) (2009).
[41] Z. Diao, D. Campanini, L. Fang, W.-K. Kwok, U. Welp, and A. Rydh, Phys. Rev. B **93**, 014509 (2016).
[42] L. Chauviére, Y. Gallais, M. Cazayous, M. A. Méasson, A. Sacuto, D. Colson, and A. Forget, Phys. Rev. B **82**, 180521(R) (2010).
[43] H. Zhai, F. Wang, and D.-H. Lee, Phys. Rev. B **80**, 064517 (2009).
[44] S. A. Hartnoll, R. Mahajan, M. Punk, and S. Sachdev, Phys. Rev. B **89**, 155130 (2014).
[45] S. Onari and H. Kontani, Phys. Rev. Lett. **109**, 137001 (2012).
[46] H. Yamase and R. Zeyher, Phys. Rev. B **88**, 125120 (2013).
[47] R. M. Fernandes, A. V. Chubukov, and J. Schmalian, Nat. Phys. **10**, 97 (2014).
[48] U. Karahasanovic, F. Kretzschmar, T. Böhm, R. Hackl, I. Paul, Y. Gallais, and J. Schmalian, Phys. Rev. B **92**, 075134 (2015).
[49] A. Hinojosa, J. Cai, and A. V. Chubukov, Phys. Rev. B **93**, 075106 (2016).